

Weakly nonlinear analysis of viscous instability in flow past a neo-Hookean surface

Paresh Chokshi and V. Kumaran

Department of Chemical Engineering, Indian Institute of Science, Bangalore 560 012, India

(Received 24 September 2007; published 8 May 2008)

We analyze the stability of the plane Couette flow of a Newtonian fluid past an incompressible deformable solid in the creeping flow limit where the viscous stresses in the fluid (of the order $\eta_f V/R$) are comparable with the elastic stresses in the solid (of the order G). Here, η_f is the fluid viscosity, V is the top-plate velocity, R is the channel width, and G is the shear modulus of the elastic solid. For $(\eta_f V/GR)=O(1)$, the flexible solid undergoes finite deformations and is, therefore, appropriately modeled as a neo-Hookean solid of finite thickness which is grafted to a rigid plate at the bottom. Both linear as well as weakly nonlinear stability analyses are carried out to investigate the viscous instability and the effect of nonlinear rheology of solid on the instability. Previous linear stability studies have predicted an instability as the dimensionless shear rate $\Gamma=(\eta_f V/GR)$ is increased beyond the critical value Γ_c . The role of viscous dissipation in the solid medium on the stability behavior is examined. The effect of solid-to-fluid viscosity ratio η_r on the critical shear rate Γ_c for the neo-Hookean model is very different from that for the linear viscoelastic model. Whereas the linear elastic model predicts that there is no instability for $H < \sqrt{\eta_r}$, the neo-Hookean model predicts an instability for all values of η_r and H . The value of Γ_c increases upon increasing η_r from zero up to $\sqrt{\eta_r}/H \approx 1$, at which point the value of Γ_c attains a peak and any further increase in η_r results in a decrease in Γ_c . The weakly nonlinear analysis indicated that the bifurcation is subcritical for most values of H when $\eta_r=0$. However, upon increasing η_r , there is a crossover from subcritical to supercritical bifurcation for $\sqrt{\eta_r}/H \approx 1$. Another crossover is observed as the bifurcation again becomes subcritical at large values of η_r . A plot in H versus $\sqrt{\eta_r}/H$ space is constructed to mark the regions where the bifurcation is subcritical and supercritical. The equilibrium amplitude and some physical quantities of interest, such as the total strain energy of the disturbance in the solid, have been calculated, and the effect of parameters H , η_r , and interfacial tension on these quantities are analyzed.

DOI: [10.1103/PhysRevE.77.056303](https://doi.org/10.1103/PhysRevE.77.056303)

PACS number(s): 47.15.Fe

I. INTRODUCTION

The flow past flexible surfaces in the low Reynolds number limit has become increasingly important in microfluidic applications, where the Reynolds number is low due to the small dimensions of the system. Due to the large surface area to volume ratio at small dimensions, the drag force per unit volume of fluid transported is much larger than that for macroscale applications. In a creeping flow, mass and heat transfer take place due to diffusion since convective effects are negligible, and it is of interest to examine the methods by which the transfer rates could be increased for efficient transport. The instability induced by the flow past a flexible surface is a possible candidate, since this could induce surface oscillations and secondary flows which could increase transport rates. Traveling waves on a flexible surface could also be more efficient for conveying fluid than a pressure drop exerted at the ends of a channel. However, in order to utilize this instability in microfluidic applications, it is necessary to have a quantitative understanding of the critical flow rates for the realistic fluid and solid models, as well as a knowledge of the nature of the initial bifurcation. The nature of the bifurcation is especially important because a controlled transition can be achieved only if the transition is supercritical. A subcritical transition would result in a discontinuous change in the perturbation amplitude at the transition point, and the critical flow rate would be lower than that predicted by the linear stability analysis. The objective of the present analysis is to provide a comprehensive picture of the critical flow rate and the nature of the transition for the viscous flow of a

Newtonian fluid past a flexible surface using a realistic (neo-Hookean) wall model for the solid. The linear stability analysis of the flow past a neo-Hookean solid has been analyzed by Gkanis and Kumar [1] when there is no dissipation in the solid. We extend the analysis for the case where there is solid dissipation, and also carry out the weakly nonlinear analysis to determine the nature of the bifurcation over a wide range of parameters.

The dynamics of fluid flow past a compliant surface is qualitatively different from that past a rigid surface due to the elasticity of the wall and the dynamical coupling between the fluid and the flexible wall medium. In particular, this coupling could influence the transition from laminar to turbulent flow. The experiments by Krindel and Silberberg, who studied the flow of a Newtonian fluid in a gel-walled tube, showed that the drag force in a flexible tube is much larger than that in a rigid tube of the same radius at a Reynolds number where the flow in a rigid tube is laminar [2]. This led them to conclude that the onset of laminar to turbulence transition in a Newtonian fluid flow through a gel-walled tube can occur at a Reynolds number much smaller than 2100, the transition Reynolds number for the flow through rigid tube. Moreover, the transition Reynolds number was influenced by the elasticity of the surface in addition to the fluid properties, indicating that the wall dynamics plays a significant role in transition. Motivated by this observation, extensive studies centered around the linear stability analysis of fluid flow in tubes and channels bounded by gel walls have been carried out [3–8].

Using the incompressible linear viscoelastic solid model for the flexible wall, Kumaran *et al.* [3] analyzed the stability

of a shear flow past a deformable solid in the low Reynolds number regime, where $Re \equiv (\rho VR / \eta_f) \ll 1$, and $(V\eta_f/GR) \sim 1$, and observed that the coupling between fluid flow and wall dynamics renders the flow unstable even in the absence of fluid inertia. Here, V is the velocity of the top plate, ρ is the density of the fluid, η_f is the viscosity of the fluid, R is the channel width, and G is the shear modulus of the solid medium. The instability, which occurs when the imposed dimensionless shear rate $\Gamma = V\eta_f/(GR)$ exceeds a certain critical value Γ_c , is driven by the discontinuity in strain rate across the fluid-solid interface. The destabilizing mechanism is proposed to be the transfer of energy from the mean flow to the fluctuations due to the shear work done by the mean flow at the interface [1–3]. The shear flow experiments conducted with a viscous fluid layer on an aqueous polymeric gel have verified the presence of an unstable mode [9–11]. A sharp increase in the apparent viscosity (calculated by assuming the flow to be laminar) was observed when the imposed shear rate exceeds a certain critical value. The experimental value of the critical shear rate required for the onset of instability was found to be in good agreement with the theoretical predictions of Kumaran *et al.* [3] for a wide range of gel thicknesses and elastic moduli. This class of modes in inertialess motion are referred to as the “viscous modes.” The analysis of viscous mode instability in flow through a flexible tube was performed by Kumaran using the linear viscoelastic constitutive model for the gel-walled tube [4].

For plane Couette flow, the displacement gradient in the deformable solid is $\Gamma = V\eta_f/GR$, which, in general, is an $O(1)$ quantity [3]. For such a case, the classical linearized theory of elasticity, which holds for small displacement gradient, is insufficient and it is imperative to incorporate the nonlinear terms in the constitutive relation for the elastic solid. This argument led Gkanis and Kumar [1] to analyze the viscous mode instability using the more appropriate neo-Hookean elastic model for the flexible surface. The neo-Hookean model is a generalization of the classical linear constitutive equation valid of finite displacement gradients, featuring additional terms nonlinear (quadratic) in solid strain [12,13]. The neo-Hookean constitutive model exhibits a nonzero first normal-stress difference in the base state, which is of the order Γ^2 and is absent for the linearly elastic solid. The linear stability analysis of Gkanis and Kumar for the plane Couette flow past a neo-Hookean elastic solid examined the role of finite deformations in the viscous instability [1]. They observed that the jump in the first normal-stress difference across the interface results in a shortwave instability in the absence of inertia and interfacial tension, as found by Renardy [14] for the flow of two viscoelastic fluid layers. The shortwave instability modes were absent for the linear elastic solid, as the normal-stress differences are zero for such a model. The neo-Hookean solid results in smaller values of the critical shear rate Γ_c and larger values of the critical wave number α_c , compared to the linear elastic model. The difference, however, diminishes as the ratio of solid-to-fluid thickness H increases. As shown by Gkanis and Kumar, the differences in Γ_c and α_c estimated by both the models become insignificant for solid thickness parameter $H \geq 10$ [1]. It should be noted here that as H was greater than 5 in the experiments [10], the observed critical shear rate was

found to be in good agreement with the predictions of Kumaran *et al.* [3], which uses the linear elastic model. The stability analysis of plane Couette flow past a neo-Hookean solid was extended to the pressure-driven creeping flow past nonlinearly elastic walled channels by Gkanis and Kumar [15]. The findings related to the different behavior from the linear elastic solid led to an immense interest in the analysis of a neo-Hookean solid present in various flow problems [16–18].

The above analyses of Kumaran *et al.* [3] and Gkanis and Kumar [1] were restricted to the stability of the base flow to the infinitesimal small amplitude disturbances. For linearly unstable flows, the finite amplitude nonlinear stability analysis reveals the nature of bifurcation (either *supercritical* or *subcritical*) after the onset of linear instability. In the weakly nonlinear analysis, an amplitude equation of the form $dA_1/dt = s^{(0)}A_1 + s^{(1)}A_1^2 + \dots$ is derived for the most unstable mode. Here $s^{(0)}$ is the linear growth rate and $s^{(1)}$ is the first Landau constant. The theory of weakly nonlinear analysis has been developed based on the pioneering works of Stuart [19] and Watson [20]. The theory is applicable for finite but small disturbances, so that the nonlinearities can be treated perturbatively. The flow through flexible tube and channel admits nonlinearities in the boundary conditions applied at the fluid-solid interface [21]. For the present study on the neo-Hookean solid, the nonlinear rheology of the viscoelastic solid also results in terms nonlinear in displacement gradients in the solid governing equations. A weakly nonlinear analysis for the unstable viscous mode was performed by Shankar and Kumaran [21]. They used a linear viscoelastic constitutive equation for the flexible solid and studied the bifurcation of the linear instability found by Kumaran *et al.* [3]. For “grafted gel,” where the polymer chains are anchored to the bottom wall, zero displacement conditions were applied, and the bifurcation was found to be subcritical for a wide range of parameters (η_r , the ratio of gel-to-fluid viscosity and H , the ratio of gel-to-fluid thickness). Recent experiments conducted by Eggert and Kumar with a layer of viscous fluid on the cross-linked polydimethylsiloxane (PDMS) gel in a parallel-plate rheometer appears to confirm the subcritical nature of the viscous instability [11].

The linear stability analysis of Gkanis and Kumar [1], which uses the finite strain neo-Hookean elastic model, ignores the contribution arising by the viscosity of the solid medium, and the stresses in solid are purely elastic stresses. However, the dissipative viscous stresses are significant in gel-like viscoelastic solids, and could have an important influence on the characteristics of the instability. We, therefore, carry out the linear stability analysis for the neo-Hookean solid augmented to include the viscous dissipation. The viscous stresses are modeled using an upper convected Maxwell model. Later, the weakly nonlinear stability is analyzed to examine the effect of nonlinearities present in the system on the linearly unstable modes for finite amplitude disturbances. Finally, we note here that the present analysis has been carried out using the spatial (or Eulerian) description as well as the material (or Lagrangian) description for the solid dynamics. However, in the interest of brevity, the detailed formulation is provided only in the Eulerian framework. The results from both the descriptions are ensured to be in quantitative

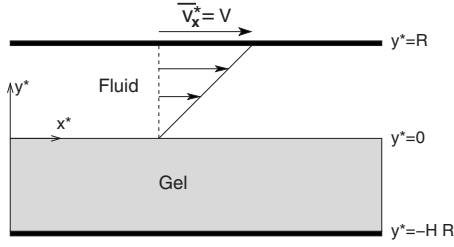


FIG. 1. Schematic diagram of plane Couette flow over a flexible surface showing the dimensional coordinate system.

agreement. The problem formulation in the Lagrangian framework is discussed briefly in the Appendix.

II. PROBLEM FORMULATION

The system consists of an incompressible Newtonian fluid of density ρ and viscosity η_f occupying the domain $0 < y^* < R$, which is supported on an incompressible viscoelastic solid medium of shear modulus G , density ρ , viscosity η_g , and thickness HR . The rigid wall at $y^* = R$ is set moving in the x direction with velocity V whereas the bottom rigid wall at $y^* = -HR$, to which the gel is grafted, is held stationary. The base flow configuration and the coordinate system are shown in Fig. 1. Here and in what follows, the quantities with a superscript $*$ are dimensional and the ones without the superscript are dimensionless unless stated otherwise. The distance is scaled with R , time with η_f/G , velocity with GR/η_f , and pressure and stresses in a fluid as well as in a gel wall are scaled with G . The scaled fluid continuity and momentum balance equations in the absence of inertia are as follows:

$$\nabla \cdot \mathbf{v} = 0, \quad (1)$$

$$\nabla \cdot \boldsymbol{\tau} = 0, \quad (2)$$

where \mathbf{v} denotes the fluid velocity field and the fluid stress tensor is of the form

$$\boldsymbol{\tau} = -p_f \mathbf{I} + [\nabla \mathbf{v} + (\nabla \mathbf{v})^T], \quad (3)$$

where p_f is the fluid pressure, \mathbf{I} is the identity tensor, and superscript T indicates the transpose.

The surface is modeled as an incompressible neo-Hookean viscoelastic solid continuum, wherein the neo-Hookean constitutive model is augmented with the viscous stresses to account for the viscous dissipation in the solid. The neo-Hookean model, which is a generalization of the linear elastic model used in the earlier analyses [3,21], is valid for a finite displacement gradient in the solid. The neo-Hookean elastic solid model has been used in the previous studies of linear stability analyses by Gkanis and Kumar [1,15], although they considered the flexible wall as an elastic solid ignored the viscous dissipation. In the Eulerian description, the dynamics of the solid wall is described by a displacement field \mathbf{u} , given by the displacement of a particle from the initial reference configuration \mathbf{X} to a configuration \mathbf{x} at any time t as

$$\mathbf{x} = \mathbf{X} + \mathbf{u}(\mathbf{x}, t). \quad (4)$$

The deformation tensor in spatial configuration is given by

$$\mathbf{f} = \frac{\partial \mathbf{X}}{\partial \mathbf{x}} = (\mathbf{I} - \nabla \mathbf{u}). \quad (5)$$

The mass conservation condition for an incompressible gel is given by either

$$\text{Det } \mathbf{f} = 1 \quad (6)$$

or

$$\nabla \cdot \mathbf{v}^g = 0, \quad (7)$$

where Det indicates the determinant and \mathbf{v}^g is the dimensionless Eulerian velocity field in the solid medium given by

$$\mathbf{v}^g = \left(\frac{\partial \mathbf{x}}{\partial t} \right)_{\mathbf{x}} = \left[\frac{\partial \mathbf{u}(\mathbf{x}(\mathbf{X}, t), t)}{\partial t} \right]_{\mathbf{x}} = \left(\frac{\partial \mathbf{u}}{\partial t} \right)_{\mathbf{x}} + \frac{\partial \mathbf{u}}{\partial \mathbf{x}} \cdot \left(\frac{\partial \mathbf{x}}{\partial t} \right)_{\mathbf{x}}, \quad (8)$$

$$\therefore \mathbf{v}^g = \partial_t \mathbf{u} + \mathbf{v}^g \cdot \nabla \mathbf{u}. \quad (9)$$

This expression in Eulerian framework is consistent with the Lagrangian expression wherein the partial time derivative of the particle position is taken. The dimensionless momentum balance equation, in the absence of inertia, is

$$\nabla \cdot \boldsymbol{\sigma} = 0. \quad (10)$$

The total stress tensor in the solid, scaled by the shear modulus G , is

$$\boldsymbol{\sigma} = -p_g \mathbf{I} + 2\mathbf{e} + \boldsymbol{\sigma}^V, \quad (11)$$

where p_g is the isotropic pressure and $\boldsymbol{\sigma}^V$ is the dissipative viscous stress tensor. The strain tensor in the neo-Hookean elastic solid is given by [12]

$$\mathbf{e} = \frac{1}{2}(\mathbf{I} - \mathbf{f}^T \cdot \mathbf{f}) \quad (12)$$

or

$$e_{ij} = \frac{1}{2} \left(\frac{\partial u_i}{\partial x_j} + \frac{\partial u_j}{\partial x_i} - \frac{\partial u_k}{\partial x_i} \frac{\partial u_k}{\partial x_j} \right). \quad (13)$$

The viscous stress tensor is described by a single relaxation time upper convective Maxwell model as follows

$$\boldsymbol{\sigma}^V + \text{De}[\partial_t \boldsymbol{\sigma}^V + \mathbf{v}^g \cdot \nabla \boldsymbol{\sigma}^V - \boldsymbol{\sigma}^V \cdot (\nabla \mathbf{v}^g) - (\nabla \mathbf{v}^g)^T \cdot \boldsymbol{\sigma}^V] = 2\eta_r \dot{\mathbf{e}}, \quad (14)$$

where the Deborah number is the solid relaxation time (λ_g) scaled with the flow time scale, $\text{De} = \lambda_g G / \eta_f$ and $\eta_r = \eta_g / \eta_f$, the ratio of solid-to-fluid viscosity. The strain rate tensor for the neo-Hookean solid is given by [12]

$$\dot{\mathbf{e}} = \frac{1}{2} [(\nabla \mathbf{v}^g)^T + \nabla \mathbf{v}^g] - [\mathbf{e} \cdot (\nabla \mathbf{v}^g)^T + \nabla \mathbf{v}^g \cdot \mathbf{e}] \quad (15)$$

or

$$\dot{e}_{ij} = \frac{1}{2} \left(\frac{\partial v_i^g}{\partial x_j} + \frac{\partial v_j^g}{\partial x_i} \right) - \left(e_{ik} \frac{\partial v_k^g}{\partial x_j} + \frac{\partial v_k^g}{\partial x_i} e_{kj} \right). \quad (16)$$

A model similar to Eq. (14) has been used by Phan-Thien [22] to describe a class of soft viscoelastic materials that includes bread dough and some biological tissues. This model incorporates both the neo-Hookean rubberlike response and the viscoelastic response modeled by a Maxwell-type equation. In the limit $De \rightarrow 0$, the viscous stress is given by the simple expression of Newton's law. Even for a finite Deborah number, the nonlinear terms in the upper convected time derivative part in the expression (14) are identically zero for the linear stability problem, because $\mathbf{v}^g = \boldsymbol{\sigma}^V = 0$ for the base state considered in the present study. The neo-Hookean elastic model is recovered in the limit $\eta_r \rightarrow 0$.

For the steady-state base flow shown in Fig. 1, the fluid velocity, the gel displacement, and the gel velocity fields are given as

$$\bar{\mathbf{v}} = (\Gamma y, 0, 0), \quad \bar{\mathbf{u}} = [\Gamma(y+H), 0, 0], \quad \bar{\mathbf{v}}^g = (0, 0, 0), \quad (17)$$

where $\Gamma = V\eta_f/(GR)$ is the dimensionless velocity of the top plate and hence is the shear rate for fluid. The stresses in the fluid and solid medium are

$$\bar{\tau}_{xx} = -\bar{p}_f, \quad \bar{\tau}_{xy} = \Gamma, \quad \bar{\tau}_{yy} = -\bar{p}_f, \quad (18)$$

$$\bar{\sigma}_{xx} = -\bar{p}_g, \quad \bar{\sigma}_{xy} = \Gamma, \quad \bar{\sigma}_{yy} = -\bar{p}_g - \Gamma^2. \quad (19)$$

In addition to the no-slip conditions $\bar{v}_x = \Gamma$ at $y=1$ and zero displacement for the grafted gel at $y=-H$, the base state also satisfies the velocity and stress continuity conditions at the fluid-solid interface, which, for the mean flow, is flat at $y=0$. The nonzero value of the first normal-stress difference $(\bar{\sigma}_{xx} - \bar{\sigma}_{yy}) = \Gamma^2$ for the elastic solid is the consequence of the finite strain neo-Hookean constitutive model. This additional stress, which was absent in the linear viscoelastic solid analysis of Ref. [3], affects the stability of the base state, especially when the shear rate $\Gamma > 1$ [1, 15].

III. WEAKLY NONLINEAR ANALYSIS

The governing equations for the solid admit terms nonlinear in displacement gradient for the neo-Hookean viscoelastic model. Moreover, the nonlinearities arise from the fluid-solid interface boundary conditions [21]. The treatment of nonlinear terms in the boundary conditions is discussed below.

A. Interface conditions

At top ($y=1$) and bottom ($y=-H$) walls, the perturbation quantities in fluid and solid, respectively, are set to be zero. At the fluid-solid interface, the tangential and normal velocities and stresses are set to be equal. While the interface in the undisturbed flow is flat at $y=0$, its position in the perturbed flow is different and it has to be obtained as a part of the solution. As illustrated schematically in Fig. 2, a material point $(x, 0)$ on the undisturbed interface moves to a position

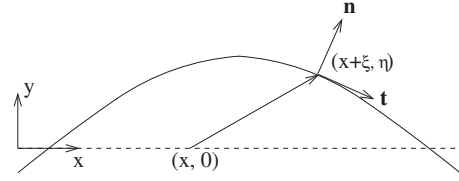


FIG. 2. Schematic illustrating the perturbed fluid-gel interface.

$(x+\xi, \eta)$ due to the perturbations, where ξ and η are Lagrangian displacement of the material point at the interface. The matching conditions at the perturbed interface are

$$(\mathbf{t} \cdot \mathbf{v})|_{x+\xi, \eta} = (\mathbf{t} \cdot \mathbf{v}^g)|_{x+\xi, \eta}, \quad (20)$$

$$(\mathbf{n} \cdot \mathbf{v})|_{x+\xi, \eta} = (\mathbf{n} \cdot \mathbf{v}^g)|_{x+\xi, \eta}, \quad (21)$$

$$(\mathbf{t} \cdot \boldsymbol{\tau} \cdot \mathbf{n})|_{x+\xi, \eta} = (\mathbf{t} \cdot \boldsymbol{\sigma} \cdot \mathbf{n})|_{x+\xi, \eta}, \quad (22)$$

$$(\mathbf{n} \cdot \boldsymbol{\tau} \cdot \mathbf{n})|_{x+\xi, \eta} = (\mathbf{n} \cdot \boldsymbol{\sigma} \cdot \mathbf{n})|_{x+\xi, \eta} + T(\nabla_s \cdot \mathbf{n})|_{x+\xi, \eta}. \quad (23)$$

Here, the scaled interfacial tension $T = \gamma/GR$, where γ is the dimensional surface tension, and ∇_s is the gradient along the interface. \mathbf{n} and \mathbf{t} are the unit vectors normal and tangent to the perturbed interface (see Fig. 2). Denoting F and G to the fluid and gel quantities, respectively, the interface conditions have the following generic form:

$$F|_{x+\xi, \eta} = G|_{x+\xi, \eta}, \quad (24)$$

where ξ and η are obtained as a part of the solution. In a weakly nonlinear analysis, the amplitudes of the perturbation quantities are assumed to be small but finite. The quantities at the perturbed interface $(x+\xi, \eta)$ can be approximated as a Taylor expansion about their values at the unperturbed interface $(x, 0)$. Thus, the generic expression of the interface conditions, Eq. (24), becomes

$$\begin{aligned} & [F]_0 + [\partial_x F]_0 \xi + [\partial_y F]_0 \eta + \frac{1}{2} [\partial_x^2 F]_0 \xi^2 + \frac{1}{2} [\partial_y^2 F]_0 \eta^2 \\ & + [\partial_x \partial_y F]_0 \xi \eta + \dots \\ & = [G]_0 + [\partial_x G]_0 \xi + [\partial_y G]_0 \eta \\ & + \frac{1}{2} [\partial_x^2 G]_0 \xi^2 + \frac{1}{2} [\partial_y^2 G]_0 \eta^2 + [\partial_x \partial_y G]_0 \xi \eta + \dots, \end{aligned} \quad (25)$$

where $[\dots]_0$ denote quantities evaluated at the unperturbed interface ($y=0$). Here ξ and η are obtained using the following Taylor expansions:

$$\begin{aligned} \xi \equiv u_x(x+\xi, \eta, t) &= [u_x]_0 + [\partial_x u_x]_0 \xi + [\partial_y u_x]_0 \eta + \frac{1}{2} [\partial_x^2 u_x]_0 \xi^2 \\ &+ \frac{1}{2} [\partial_y^2 u_x]_0 \eta^2 + [\partial_x \partial_y u_x]_0 \xi \eta + \dots, \end{aligned} \quad (26)$$

$$\begin{aligned} \eta \equiv u_y(x + \xi, \eta, t) &= [u_y]_0 + [\partial_x u_y]_0 \xi + [\partial_y u_y]_0 \eta + \frac{1}{2} [\partial_x^2 u_y]_0 \xi^2 \\ &+ \frac{1}{2} [\partial_y^2 u_y]_0 \eta^2 + [\partial_x \partial_y u_y]_0 \xi \eta + \dots \end{aligned} \quad (27)$$

The expressions for ξ and η , in terms of displacement components u_x and u_y and their derivatives evaluated at $y=0$, can be obtained from the above expansions up to the desired order of perturbation amplitude.

B. Theory

The theory of weakly nonlinear analysis is briefly discussed next. A two dimensional perturbation of small but finite amplitude $A_1(\tau)$ with axial wave number $\alpha = \alpha_c$ and frequency ω is superimposed on the base state at the critical condition. Here, τ is the slow time scale, which will be defined later. Using the definition $E(x, t) = \exp[i(\alpha x + \omega t)]$ for convenience, a general field ϕ is expanded as follows [19,20]:

$$\begin{aligned} \phi(x, y, t) &= \bar{\phi}(y) + \sum_{k=0}^{\infty} \sum_{n=k, n \neq 0}^{\infty} [A_1(\tau)]^n [E^k \bar{\phi}^{(k,n)}(y) \\ &+ E^{-k} \bar{\phi}^{(k,n)\dagger}(y)], \end{aligned} \quad (28)$$

where the overbar represents the base flow quantity and the superscript \dagger denotes the complex conjugate, and $\phi = [\mathbf{v}, p_f, \mathbf{u}, p_g, \dots]$. Here and in what follows k denotes the harmonic index and n denotes the asymptotic order. The perturbation amplitude $A_1(\tau)$, which varies on the slow time scale τ , is a small parameter and is written as $A_1(\tau) = \epsilon A(\tau)$, where ϵ is the small parameter in the expansion and $A(\tau) \sim O(1)$. It should be noted that $A_1(\tau)$ is a real quantity, since the temporal oscillations are included in $E(x, t)$.

In the vicinity of the point of critical stability such that the imposed shear rate Γ is very close to the critical shear rate Γ_c , the disturbance amplitude is assumed to satisfy the following equation known as the Landau equation:

$$A_1(\tau)^{-1} d_\tau A_1(\tau) = s_r^{(0)} + A_1(\tau)^2 s_r^{(1)} + \dots, \quad (29)$$

where the constant $s_r^{(0)}$ is the real part of the linear growth rate which emerges as an eigenvalue from the classical linearized stability analysis. The constant $s_r^{(1)}$ is the real part of the first Landau constant $s^{(1)}$. If the flow is neutrally stable to infinitesimal disturbance, which is $s_r^{(0)} = 0$, then the sign of $s_r^{(1)}$ determines the growth or decay of a weak disturbance. In the neighborhood of neutral stability such that $(\Gamma - \Gamma_c) \ll 1$, the linear growth rate can be expressed as $s_r^{(0)} = (\Gamma - \Gamma_c)(ds_r^{(0)}/d\Gamma)$. If $s_r^{(1)}$ is $O(1)$, then the second term on the right-hand side of Eq. (29) is $O(\epsilon^2)$, since $A_1(\tau) = \epsilon A(\tau)$ and the balance with the first term is achieved if $(\Gamma - \Gamma_c)(ds_r^{(0)}/d\Gamma) \sim \epsilon^2$. For definiteness, let $(\Gamma - \Gamma_c) = \Gamma_2 \epsilon^2$, where Γ_2 is $O(1)$. In order to establish a balance between the right and left sides of Eq. (29), we introduce the slow time scale τ such that the time derivative d_t is written as $d_t \rightarrow d_\tau + \epsilon^2 d_r$. Hence, there exists multiple time scales in the system: a fast time scale (t) corresponding to the inverse of the frequency of oscillations, and a slow time scale (τ) correspond-

ing to the rate of growth or decay of the disturbance amplitude. Since the $A_1(\tau)$ is independent of the fast time scale t , the scaled dynamical equation for the amplitude becomes

$$A(\tau)^{-1} d_\tau A(\tau) = \Gamma_2 \frac{ds_r^{(0)}}{d\Gamma} + A(\tau)^2 s_r^{(1)} + \dots \quad (30)$$

C. Linearized equations

The perturbation with harmonic index $k=1$ and amplitude order $n=1$ is the fundamental mode and the problem at this order corresponds to the linear stability problem. The fluid governing equations at this order for the inertialess flow are

$$i\alpha \bar{v}_x^{(1,1)} + d_y \bar{v}_y^{(1,1)} = 0, \quad (31)$$

$$-i\alpha \bar{p}_f^{(1,1)} + (d_y^2 - \alpha^2) \bar{v}_x^{(1,1)} = 0, \quad (32)$$

$$-d_y \bar{p}_f^{(1,1)} + (d_y^2 - \alpha^2) \bar{v}_y^{(1,1)} = 0, \quad (33)$$

where $d_y = d/dy$. The mass and momentum conservation equations for the neo-Hookean solid are

$$i\alpha \bar{u}_x^{(1,1)} + i\alpha \Gamma \bar{u}_y^{(1,1)} + d_y \bar{u}_y^{(1,1)} = 0, \quad (34)$$

$$\begin{aligned} -i\alpha \bar{p}_g^{(1,1)} + (1 + s^{(0)} \eta_{\text{eff}}) [(d_y^2 - \alpha^2) \bar{u}_x^{(1,1)} - i\alpha \Gamma d_y \bar{u}_x^{(1,1)} \\ + \alpha^2 \Gamma \bar{u}_y^{(1,1)}] = 0, \end{aligned} \quad (35)$$

$$\begin{aligned} -d_y \bar{p}_g^{(1,1)} + (1 + s^{(0)} \eta_{\text{eff}}) [(d_y^2 - \alpha^2) \bar{u}_y^{(1,1)} - i\alpha \Gamma d_y \bar{u}_y^{(1,1)} \\ + \alpha^2 \Gamma \bar{u}_x^{(1,1)} - 2\Gamma d_y^2 \bar{u}_x^{(1,1)}] = 0, \end{aligned} \quad (36)$$

where $s^{(0)}$ is the complex-valued linear growth rate and the effective solid viscosity η_{eff} is given by the expression $\eta_{\text{eff}} = \eta_r / (1 + s^{(0)} \text{De})$. Here, De is the Deborah number for the solid and $\eta_r = \eta_g / \eta_f$, the ratio of solid-to-fluid viscosity.

The boundary conditions for this problem include the vanishing eigenfunctions at the top and bottom plates and the interface conditions. At the perturbed fluid-solid interface, the Taylor expansion of the matching conditions results in the following equalities to be enforced at $y=0$:

$$\bar{v}_y^{(1,1)} = s^{(0)} \bar{u}_y^{(1,1)}, \quad (37)$$

$$\bar{v}_x^{(1,1)} + \Gamma \bar{u}_y^{(1,1)} = s^{(0)} \bar{u}_x^{(1,1)} + s^{(0)} \Gamma \bar{u}_y^{(1,1)}, \quad (38)$$

$$\begin{aligned} d_y \bar{v}_x^{(1,1)} + i\alpha \bar{v}_y^{(1,1)} = (1 + s^{(0)} \eta_{\text{eff}}) (d_y \bar{u}_x^{(1,1)} + i\alpha \bar{u}_y^{(1,1)} - i\alpha \Gamma \bar{u}_x^{(1,1)}) \\ - i\alpha \Gamma^2 \bar{u}_y^{(1,1)}, \end{aligned} \quad (39)$$

$$\begin{aligned} -\bar{p}_f^{(1,1)} + 2d_y \bar{v}_y^{(1,1)} = -\bar{p}_g^{(1,1)} + 2(1 + s^{(0)} \eta_{\text{eff}}) \\ \times (d_y \bar{u}_y^{(1,1)} - \Gamma d_y \bar{u}_x^{(1,1)}) + T \alpha^2 \bar{u}_y^{(1,1)}. \end{aligned} \quad (40)$$

Equation (37) is the normal-velocity continuity condition at the fluid-solid interface. Equation (38) gives the tangential-velocity continuity condition, wherein the second term on the left-hand side is due to a jump in mean flow shear rate across the interface and the right-hand side is the expression for the

Eulerian velocity field in the solid which contains a base-fluctuation coupling term due to a finite displacement gradient in the base state. The tangential-stress continuity is given by Eq. (39). Here, the last term on the right-hand side is due to the normal-stress difference in the solid. As shown in Sec. II, the neo-Hookean solid exhibits the first normal-stress difference $(\bar{\sigma}_{xx} - \bar{\sigma}_{yy}) = \Gamma^2$ in the base state. This normal-stress difference contributes to the perturbation tangential stress due to nonflat interface. Equation (40) is the normal-stress continuity condition, wherein the term containing T is the surface force due to nonzero interfacial tension T . It should be noted that, all the terms containing Γ on the right-hand side of the above conditions are due to the neo-Hookean nature of the solid medium. These terms were absent for the linear viscoelastic gel model used in the analysis of Kumaran *et al.* [3].

The fluid and solid governing equations [(31)–(36)] are solved analytically to give solutions for the normal component as follows:

$$\tilde{v}_y^{(1,1)} = A_1 e^{-\alpha y} + A_2 y e^{-\alpha y} + A_3 e^{\alpha y} + A_4 y e^{-\alpha y}, \quad (41)$$

$$\tilde{u}_y^{(1,1)} = B_1 e^{-\alpha y} + B_2 e^{(\alpha - i\alpha\Gamma)y} + B_3 e^{-(\alpha + i\alpha\Gamma)y} + B_4 e^{\alpha y}. \quad (42)$$

The eigenfunctions satisfy the no-slip conditions at the top and bottom plates as follows:

$$\tilde{v}_y^{(1,1)} = \tilde{v}_x^{(1,1)} = 0 \quad \text{at } y = +1, \quad (43)$$

$$\tilde{u}_y^{(1,1)} = \tilde{u}_x^{(1,1)} = 0 \quad \text{at } y = -H. \quad (44)$$

Upon substituting the expressions (41) and (42) in the above stated boundary conditions and the interface conditions (37)–(40), we obtain a matrix equation of the form

$$\mathbf{M}\mathbf{a} = \mathbf{0}, \quad (45)$$

where \mathbf{M} is an 8×8 dispersion matrix and $\mathbf{a} = [A_1 A_2 A_3 A_4 B_1 B_2 B_3 B_4]^T$. The nontrivial solutions exist for a set of complex eigenvalues $s^{(0)}$. The characteristic equation of matrix \mathbf{M} gives a dispersion relation for the eigenvalue in terms of the flow parameters. For neutral stability, the transition value of shear rate Γ_t is obtained by setting the real part of growth rate $s_r^{(0)}$ to zero. The point of critical stability is then obtained by locating a point of minimum Γ_t on a neutral stability curve in the α - Γ_t plane. To determine the eigenfunctions, an additional ‘‘normalization’’ condition is required, which we specify here as $\tilde{v}_y^{(1,1)}|_{y=0} = (1+i)$. The equivalent governing equations in the Lagrangian framework are given in the Appendix.

D. Calculation of the Landau constant $s^{(1)}$

The objective of the rest of the analysis is to determine the first Landau constant $s^{(1)}$, which in turn determines whether the nature of viscous instability is supercritical or subcritical. Upon expanding all the dynamical quantities in a harmonic-amplitude series, as shown in a Eq. (28), and extracting the governing equations at various orders, inhomogeneous terms appear in the solid governing equations due to the nonlinearities in the rheological model. Moreover, the

interfacial conditions at the perturbed interface, which are written in Taylor series expansion about the flat interface as in Eq. (25), introduce nonlinearities. In general, the problem at order (k, n) contains inhomogeneous terms of order (j, m) , where $m < n$ and $j + m \leq k + n$. In the hierarchy of problems at various orders, the first Landau constant $s^{(1)}$ first appears in the problem with $k=1$ and $n=3$. Therefore, in the weakly nonlinear analysis, where the objective is to calculate only the first constant $s^{(1)}$, only few selected problems at orders $(1, 1)$, $(0, 2)$, $(2, 2)$, and $(1, 3)$ need to be solved necessarily in that order. The $(1, 1)$ problem is the linear stability analysis which provides the critical point around which the harmonic-amplitude expansion is carried out, the $(0, 2)$ problem is the A_1^2 correction to the mean flow, often termed as the base flow distortion, the $(2, 2)$ problem is the first harmonic of the fundamental mode which manifests at order A_1^2 , and the $(1, 3)$ problem is the nonlinear correction to the least stable fundamental mode, at which order the Landau equation is recovered.

The governing equations and the interface conditions for the $(0, 2)$ and $(2, 2)$ problems are similar to the expressions (31)–(40) for the $(1, 1)$ problem with wave number α being replaced with 0 and 2α , respectively. In addition, inhomogeneous terms containing the eigenfunctions of the $(1, 1)$ problem appear on the right-hand sides of the governing equations for solid dynamics and the interface conditions, arising due to the nonlinearities present in the neo-Hookean constitutive relation and the Taylor expansion about the perturbed interface respectively. The equations for the fluid and solid media can be solved analytically using MATHEMATICA. Upon substituting the solutions in the boundary and interface conditions, we get a matrix problem of the form

$$\mathbf{M}^{(k,n)}\mathbf{a} = \boldsymbol{\gamma}^{(k,n)}, \quad (46)$$

where \mathbf{a} is a vector of constants and $\boldsymbol{\gamma}^{(k,n)}$ is the inhomogeneous part known in terms of the fundamental mode $(1, 1)$. Here, $\mathbf{M}^{(k,n)}$ is a nonsingular matrix. The solution of this linear system of equations exists as matrix $\mathbf{M}^{(k,n)}$ is invertible for the $(0, 2)$ and $(2, 2)$ problems. For the $(1, 3)$ problem, the matrix operator $\mathbf{M}^{(1,3)}$ is identical to that in the expression (45) for the linear problem ($k=1, n=1$), and hence is singular. The nontrivial solution of the inhomogeneous $(1, 3)$ problem, therefore, necessitates the Fredholm solvability criterion to be satisfied. In order to formulate the solvability criterion, we need the solution of the homogeneous adjoint problem. The adjoint problem is constructed by defining the inner product of two vectors $\boldsymbol{\phi}$ and $\boldsymbol{\psi}$ as

$$\langle \boldsymbol{\phi}, \boldsymbol{\psi} \rangle = \sum_i \phi_i^\dagger \psi_i, \quad (47)$$

where ϕ_i^\dagger is the complex conjugate of ϕ_i . The homogeneous adjoint problem of the original problem $\mathbf{M}\mathbf{a} = \boldsymbol{\gamma}^{(1,3)}$ is given as

$$\mathbf{M}^* \boldsymbol{\psi} = \mathbf{0}, \quad (48)$$

where $M_{ij}^* = M_{ji}^\dagger$ is the adjoint of matrix \mathbf{M} and $\boldsymbol{\psi}$ is the nontrivial solution for the homogeneous adjoint problem which can be obtained using any additional condition on vector $\boldsymbol{\psi}$.

The Fredholm solvability criterion is to make ψ orthogonal to the inhomogeneity vector $\gamma^{(1,3)}$ as follows:

$$\langle \psi, \gamma^{(1,3)} \rangle = 0. \quad (49)$$

The inhomogeneous part $\gamma^{(1,3)}$ contains the first Landau constant, consequently, the solvability condition (49) gives the numerical value of the Landau constant $s^{(1)}$. A detailed discussion on the solution procedure can be found in Thakkar and Kumaran [23].

IV. RESULTS AND DISCUSSIONS

A. Linear stability analysis

For a flow past a neo-Hookean solid, the stability of the base state to the infinitesimal amplitude disturbances was analyzed by Gkanis and Kumar [1]. They considered a solid medium which is purely elastic in nature ignoring the viscous dissipation of the disturbance energy, and elucidated the salient features of the finite strain neo-Hookean model that are different from the analysis of Kumaran *et al.* [3] for the linearly elastic surface. We first recall the results of the linear stability analysis performed for a neo-Hookean solid surface in the absence of viscous dissipation, and then study the effect of viscosity of the solid medium on the critical parameter.

In addition to the finite wave-number instability qualitatively similar to the one present in the linear elastic solid, the neo-Hookean model exhibits the shortwave mode of instability arising due to a nonzero first normal-stress difference in the elastic medium. This normal-stress difference in the base state, $(\bar{\sigma}_{xx} - \bar{\sigma}_{yy}) = \Gamma^2$, results in a jump in the first normal-stress difference across the fluid-solid interface, which is known to excite a shortwave instability at the interface [14]. While the shortwave instability is present for all values of solid thickness H and is independent of H for $H \gg 1$, this mode of instability is critical, in comparison to the finite wave-number mode, only for thin solids with $H \leq 1.2$. For relatively thick solids, the instability is excited by the finite wave-number mode. It should be noted here that the wave speed of the shortwave instability mode is negative. Therefore, the large wave-number modes are upstream traveling waves, whereas the finite wave-number modes, like the unstable modes for the linear elastic solid, are downstream traveling waves. The variations of the critical shear rate Γ_c for the onset of instability, and the critical wave number α_c , with the dimensionless solid thickness H are shown in Fig. 3 for $\eta_r = 0$. This plot is the same as the one reported in Ref. [1] and is shown because the weakly nonlinear analysis is carried out at the critical points (α_c, Γ_c) along this plot. As seen for $T=0$, Γ_c is independent of H for $H \leq 1.2$, reflecting the shortwave instability. A very high value of α_c for this case further confirms the shortwave nature of the instability. The value of Γ_c for the neo-Hookean model is lower than its value for the linear elastic solid and the difference becomes significant for $H < 1$. The discrepancy between the two models for small H is attributed to the additional finite strain terms in the neo-Hookean model which are proportional to the base-state strain Γ , and also the first normal stress which

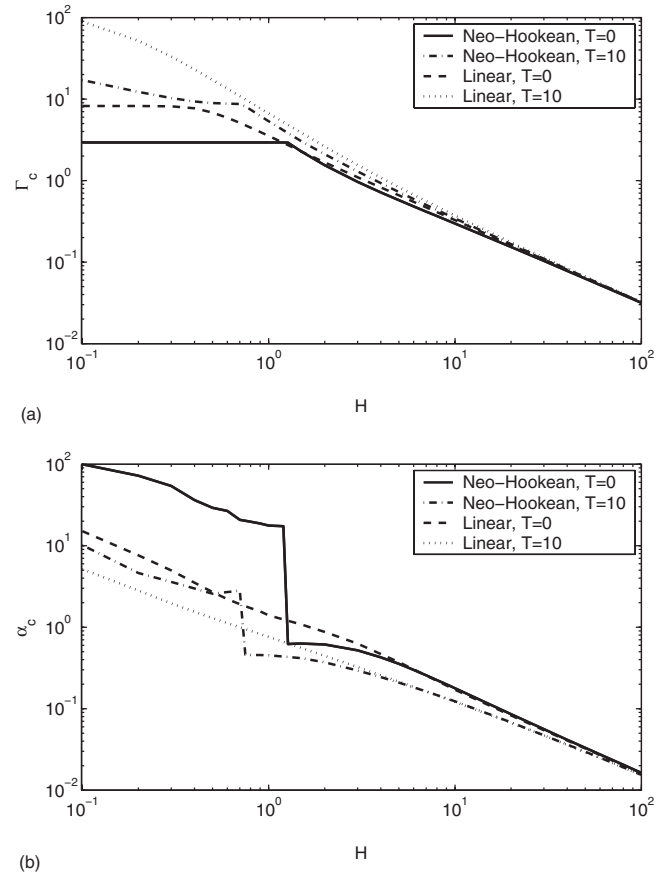


FIG. 3. Effect of solid thickness H on (a) the critical shear rate Γ_c , and (b) the critical wave number α_c , for $\eta_r = 0$. Results are plotted for both the neo-Hookean as well as the linear elastic models.

is of the order Γ^2 . As observed, the effect of these additional stresses is destabilizing. However, for large H , the value of Γ_c is lower than unity and hence, the contribution of the additional stresses becomes insignificant. Consequently, both the results converge in the limit of large H ($H > 10$). The figure also shows the stabilizing influence of the interfacial tension, as an increase in interfacial tension increases Γ_c and reduces α_c . In the limit $H \gg 1$, the critical shear rate Γ_c , and the wave-number α_c , decrease proportional to H^{-1} . In this limit, the characteristics of the most unstable mode are independent of T because the wavelength of the fastest growing mode increases proportional to H for $H \gg 1$ and the stress generated due to interfacial tension decreases as the wavelength increases.

Next, we take into consideration the viscous part of the solid stresses by setting a nonzero value to η_r , the ratio of solid-to-fluid viscosity. Before we discuss the results for the neo-Hookean viscoelastic solid, it will be beneficial to recall the results for the linearly viscoelastic solid analyzed by Kumaran *et al.* [3]. They observed that the gel viscosity has a stabilizing influence on the unstable mode, and the flow could become stable for all values of Γ if η_r is sufficiently high. For $\eta_r > 1$, while there are unstable traveling modes for $H > \sqrt{\eta_r}$, the interface was found to be stable for $H < \sqrt{\eta_r}$. The critical shear rate Γ_c diverges proportional to

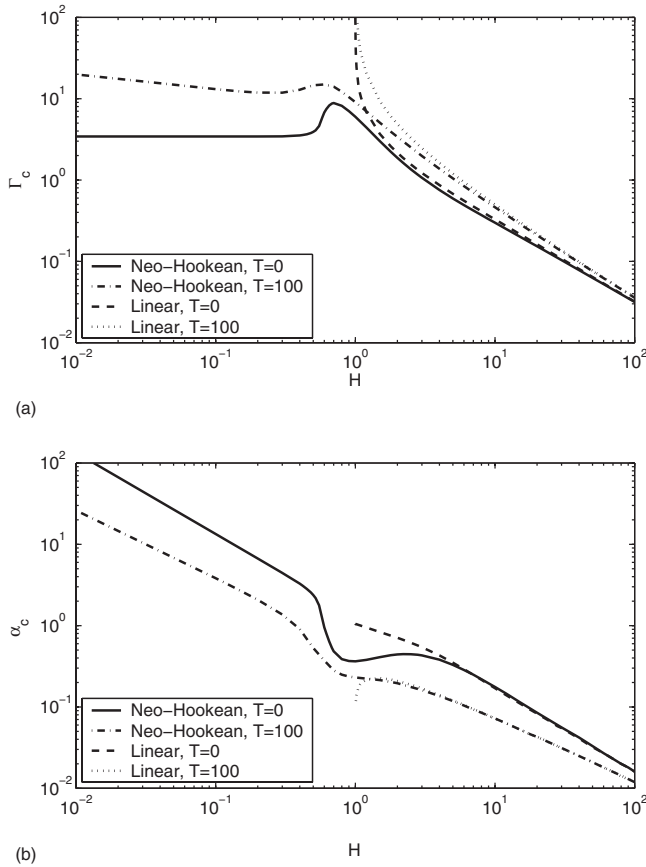


FIG. 4. Effect of solid thickness on the critical shear rate Γ_c and the critical wave number α_c for $\eta_r=1$. Results are plotted for both the neo-Hookean as well as the linear elastic models.

$(H - \sqrt{\eta_r})^{-1}$ independent of the interfacial tension T as H approaches $\sqrt{\eta_r}$. For $\eta_r=1$, there are no unstable modes for $H < 1$ and the critical shear rate diverges as $\Gamma_c \propto (H-1)^{-1/2}$ for $T=0$ and $\Gamma_c \propto T^{1/4}(H-1)^{-3/4}$ for $T \neq 0$ in the limit $H \rightarrow 1$. For $\eta_r < 1$ (which includes the case $\eta_r=0$), the instability was found to persist for all values of H . In the present study, the neo-Hookean elastic model is augmented to include the viscous dissipation in the solid. The viscous stresses are modeled using a Maxwell-type equation [Eq. (14)] with Deborah number De as the dimensionless relaxation time in the solid. For dissipating solids with $\eta_r=1$, Fig. 4 shows the critical shear rate as a function of H keeping $De=0$. For the linear viscoelastic model, Γ_c diverges in the limit $H \rightarrow 1$ and the instability disappears for $H < 1$. However, for the neo-Hookean model, the instability does persist for $H < 1$. A peak in Γ_c is observed at H around 1. At this point, the additional stresses due to the finite deformations, including the first normal-stress difference jump, become important, and these terms are destabilizing. Therefore, an instability is observed for all values of H in the neo-Hookean model.

In Fig. 5, we plot $\Gamma_c H$ as a function of $\sqrt{\eta_r}/H$ for different values of H . This figure shows that for neo-Hookean solid, the unstable traveling waves exist even for $\sqrt{\eta_r}/H > 1$. An important thing to note here is that while all the curves with different H collapse onto a single curve for $\sqrt{\eta_r}/H < 1$, such a behavior is not observed for the case $\sqrt{\eta_r}/H > 1$. That

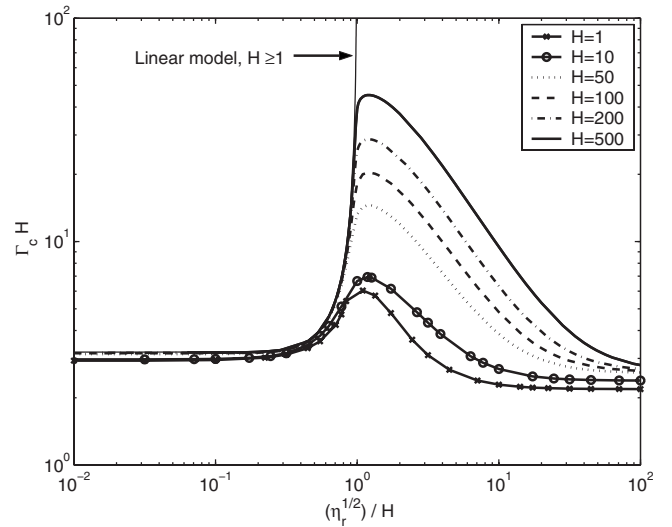


FIG. 5. Effect of η_r on Γ_c plotted on the scaled coordinates $\Gamma_c H$ versus $\sqrt{\eta_r}/H$ for different values of H keeping $De=0$ and $T=0$. The curve for the linear elastic model is also shown for comparison as a thin line.

means, in the later case, the scaling $\Gamma_c \sim H^{-1}$ for $H \gg 1$ does not hold. The peak value of Γ_c for different H was found to follow the scaling $\Gamma_c \sim H^{-1/2}$ at $\sqrt{\eta_r}/H \approx 1$ for $H \gg 1$. Interestingly, η_r has opposite effects in two different regimes. While increasing η_r has a stabilizing influence on Γ_c in the regime $\sqrt{\eta_r}/H < 1$, the influence is destabilizing (as an increase in η_r tends to reduce Γ_c) in the regime $\sqrt{\eta_r}/H > 1$. This opposing effect of η_r on both the sides of $\sqrt{\eta_r}/H \approx 1$ is specific to the neo-Hookean constitutive equation for strain rate tensor, and is not present in the linear viscoelastic model. For the linear stability analysis, the effect of the Deborah number is to merely modify the relative solid viscosity η_r . Figure 6 indicates the influence of the Deborah number on the critical shear rate for the dissipative solids. It is seen that the plot does not change significantly

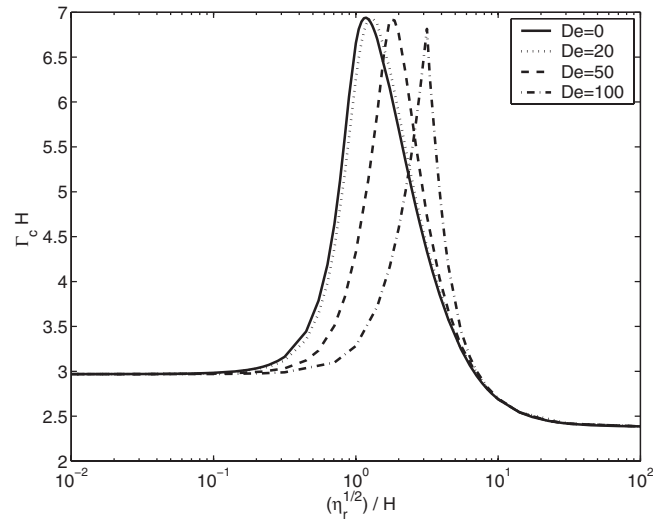


FIG. 6. Effect of η_r on Γ_c plotted on the scaled coordinates $\Gamma_c H$ versus $\sqrt{\eta_r}/H$ for different values of De for $H=10$ and $T=0$.

TABLE I. The first Landau constant $s^{(1)}$ computed at the critical point for the neo-Hookean elastic solid model for different values of solid thickness H keeping $\eta_r=0$ and $T=0$.

H	α_c	Γ_c	$s_i^{(0)}$	$(ds_r^{(0)}/d\Gamma)$	Real[$s^{(1)}$]	Imag[$s^{(1)}$]
0.10	100.0	2.93114248	1.00000000	0.1607566850	253529.143	56714.095
0.20	72.20	2.93114246	1.00000000	0.1608037980	132128.055	29353.215
0.30	54.00	2.93114246	1.00000000	0.1608585720	73860.463	16262.874
0.40	36.30	2.93114246	1.00000000	0.1609915970	33329.364	7208.7300
0.50	29.20	2.93114246	1.00000000	0.1609877120	21546.593	4599.1451
0.60	26.70	2.93114246	1.00000000	0.1609931850	18006.394	3818.8800
0.80	19.67	2.93114246	1.00000000	0.1609867470	9753.8680	2013.0878
1.00	17.64	2.93114246	1.00000000	0.1609887520	7837.8850	1598.3704
1.20	17.34	2.93114246	1.00000000	0.1609900900	7572.5541	1540.9946
1.27	0.620	2.91813557	-0.36719925	0.0294114167	-18.5149687	-43.2588194
1.30	0.623	2.81416097	-0.36527716	0.0305992269	-15.6100164	-40.8074391
1.50	0.630	2.27140715	-0.34478723	0.0384902983	-2.0288370	-29.2209990
2.00	0.614	1.54046549	-0.28190573	0.0508989795	11.7108298	-15.2426429
3.00	0.520	0.96301788	-0.18368174	0.0525905941	22.3395167	-6.6097654
4.00	0.427	0.71500641	-0.12418385	0.0428700141	30.7389377	-3.8965707
5.00	0.355	0.57410443	-0.08789064	0.0329721252	39.7070800	-3.2991380
6.00	0.299	0.48183541	-0.06441809	0.0249954162	49.8670434	-4.3588286
10.00	0.178	0.29680357	-0.02508044	0.0098615917	92.1882493	-22.1699354
20.00	0.0856	0.15305103	-0.00641943	0.0024102192	172.452899	-95.6796243
50.00	0.0331	0.06268374	-0.00103038	0.0003682593	362.255355	-293.713077
80.00	0.0205	0.03943620	-0.00040258	0.0001417991	549.009042	-480.554217
100.0	0.0163	0.03162049	-0.00025688	8.9826×10^{-5}	674.548152	-612.078718
200.0	0.0081	0.01588353	-6.423×10^{-5}	2.2227×10^{-5}	1298.72791	-1233.12174
500.0	0.0032	0.00637168	-1.019×10^{-5}	3.4818×10^{-6}	3175.16521	-3204.61388
1000	0.0016	0.00318887	-2.550×10^{-6}	8.7040×10^{-7}	6300.04658	-6379.19398

for $De=0-20$. For a Deborah number larger than 20, the numerical value of Γ_c varies, but the qualitative nature of the graph remains unchanged.

B. Weakly nonlinear stability analysis

For a nondissipative neo-Hookean solid with $\eta_r=0$, we calculate the first Landau constant $s^{(1)}$ for the critical shear rate Γ_c versus H curve shown earlier in Fig. 3 for $T=0$. The results for few points along the curve are tabulated in Table I. As mentioned before, up to $H=1.2$, the shortwave instability is critical, which is also seen by the large value of α_c and the positive sign of linear frequency $s_i^{(0)}$. The real part of the first Landau constant $s_r^{(1)}$ is found to be large positive for the shortwave instability mode, indicating the subcritical nature of the bifurcation. For $H > 1.2$, when the finite wave-number mode becomes critical, $s_r^{(1)}$ is negative at first, becomes positive, and then increases monotonously as the solid thickness increases. For comparison with the linear viscoelastic model, we recall the results of the weakly nonlinear analysis of Shankar and Kumaran [21]. They found the bifurcation to be subcritical, as the real part of the first Landau constant was always positive for a wide range of parameters H and η_r . Our estimation of $s_r^{(1)}$ for neo-Hookean solid differs significantly from the Hookean results for small H . However, as H in-

creases beyond 10, the values of $s_r^{(1)}$ given in Table I are found to agree more closely with the results reported in Ref. [21].

An important quantity in a nonlinear stability analysis is the equilibrium amplitude for which the linear growth rate and its nonlinear correction balance each other in the neighborhood of the critical point. The scaled Landau equation near $\Gamma=\Gamma_c$ is given in Sec. III [Eq. (30)]. The equilibrium amplitude, obtained by setting $dA/d\tau=0$, is given by

$$A_e^2 = \frac{-(ds_r^{(0)}/d\Gamma)\Gamma_2}{s_r^{(1)}}. \quad (50)$$

Noting that the actual amplitude $A_1 = \epsilon A$ and $(\Gamma - \Gamma_c) = \epsilon^2 \Gamma_2$,

$$A_{1e}^2 = \frac{(ds_r^{(0)}/d\Gamma)(\Gamma_c - \Gamma)}{s_r^{(1)}}. \quad (51)$$

For $s_r^{(1)} > 0$, amplitude A_{1e}^2 is positive for $\Gamma < \Gamma_c$, and for $s_r^{(1)} < 0$, the positive amplitude exists for $\Gamma > \Gamma_c$. It is important to note here that the numerical values of the Landau constant, and hence the values of A_{1e}^2 , depend upon the normalization condition used to obtain the eigenfunctions in the linear stability problem. In the present study, the normalization condition $\tilde{v}_y^{(1,1)} = (1+i)$ at $y=0$ has been used. However,

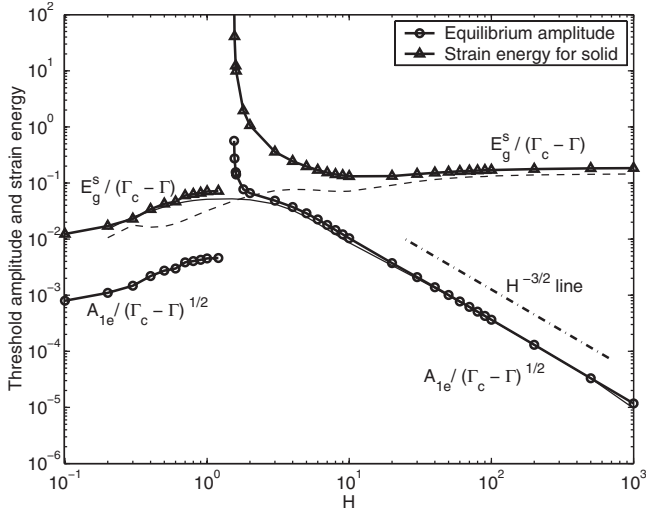


FIG. 7. Variation of the equilibrium amplitude $A_{1e}/\sqrt{\Gamma_c - \Gamma}$ and total strain energy for the solid $E_g^s/(\Gamma_c - \Gamma)$ with solid thickness for $\eta_r=0$ and $T=0$. The results for the linearly elastic solid model are also plotted as thin lines without marker. For the neo-Hookean case, the threshold amplitude and energy are plotted only when the bifurcation is subcritical ($s_r^{(1)} > 0$).

any perturbation quantity of the form $A_{1e} \tilde{\phi}(y) e^{i(ax+s^{(0)}t)}$ will be independent of the normalization condition employed. A quantity, such as the energy of the perturbations, can be determined in terms of the equilibrium amplitude. The rate of work done at the fluid-solid interface, which is given by the expression $\int_{\mathcal{A}} (\mathbf{n} \cdot \boldsymbol{\tau} \cdot \mathbf{v} + \mathbf{n} \cdot \boldsymbol{\sigma} \cdot \mathbf{v}^s) dA$, where \mathcal{A} is the surface area of the interface, is the power input to the disturbance energy. In general, a part of this deformation work is dissipated in the fluid and the solid domain, while the remaining is stored as the elastic strain energy of deformation and the kinetic energy of the fluid [4]. For the flow in the limit of zero Reynolds number, the disturbance kinetic energy is insignificant compared to the strain energy of elastic solid which is defined as

$$E_g^s = \frac{A_{1e}^2}{2} \int_{-H}^0 \tilde{\boldsymbol{\sigma}}_e^{(1,1)} : \tilde{\mathbf{e}}^{(1,1)} dy. \quad (52)$$

For a subcritically unstable flow, this energy represents the threshold energy required for destabilizing the system when the strain rate is below the transition value. Figure 7 shows the equilibrium amplitude and the threshold strain energy in the forms $A_{1e}/\sqrt{\Gamma_c - \Gamma}$ and $E_g^s/(\Gamma_c - \Gamma)$ as a function of the solid thickness H for $\eta_r=0$ and $T=0$. The threshold quantities are plotted only for the case when the bifurcation is subcritical ($s_r^{(1)} > 0$), and the curves are not shown for the narrow region where the bifurcation is supercritical ($s_r^{(1)} < 0$). The equilibrium amplitude, and hence the energy, diverge when $s_r^{(1)}$ becomes zero. The thin lined curves correspond to the equilibrium amplitude (solid line) and the threshold energy (broken line) for the linearly elastic model, for which the bifurcation is always subcritical. The results obtained for both the models agree well with each other in the limit $H \gg 1$. As seen from the figure, the threshold strain

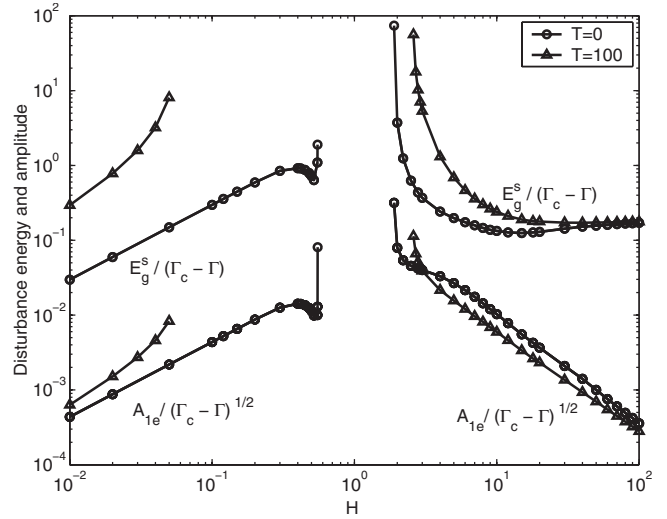


FIG. 8. Variation of the equilibrium amplitude $A_{1e}/\sqrt{\Gamma_c - \Gamma}$ and strain energy for the solid $E_g^s/(\Gamma_c - \Gamma)$ with solid thickness H for $\eta_r=1$ and $De=0$. Here, the threshold amplitude and energy are plotted only when the bifurcation is subcritical ($s_r^{(1)} > 0$).

energy corresponding to the shortwave instability (which is critical for $H \leq 1.2$) is lower by an order of magnitude than that corresponding to the finite wave-number instability (which is the critical mode of instability for $H > 1.2$). The shortwave instability modes are, therefore, highly subcritical in nature, which is evident from the large values of the first Landau constant for these modes (see Table I). Figure 8 shows the variation of the threshold amplitude and the elastic strain energy with H for the dissipative solid with $\eta_r=1$ and two different values of T . For thin solids, when the critical mode of instability is of shortwave nature, the interfacial tension tends to increase the threshold strain energy for a finite amplitude instability, indicating the stabilizing influence of the interfacial tension on shortwave instability. Further, for a nonzero interfacial tension, the region of supercritical stability near $H \approx 1$ becomes wider in comparison to the case with $T=0$.

The effect of η_r , the solid-to-fluid viscosity ratio, on the first Landau constant is reflected in Fig. 9, where the threshold energy and the equilibrium amplitude are plotted against the scaled quantity $\sqrt{\eta_r}/H$ for the cases $H=10$, $T=10$, and $De=0$. Here, the full lines represent the energy $E_g^s/(\Gamma_c - \Gamma)$, and the amplitude square $A_{1e}^2/\sqrt{\Gamma_c - \Gamma}$, for the subcritical bifurcation, and the broken lines show the energy $E_g^s/(\Gamma - \Gamma_c)$ and the amplitude $A_{1e}/\sqrt{\Gamma - \Gamma_c}$, when the bifurcation is supercritical. Upon increasing η_r from $\eta_r=0$, the effect of η_r is to decrease $s_r^{(1)}$, which changes its sign from positive to negative, resulting in a crossover of bifurcation from subcritical to supercritical. This crossover, which occurs when $s_r^{(1)}$ becomes zero, is observed at $\sqrt{\eta_r}/H \approx 1$. For larger values of η_r , the effect of solid viscosity is destabilizing, as the nonlinear effects undergo a change from supercritical to subcritical bifurcation near $\sqrt{\eta_r}/H \approx 6$.

Another quantity of interest in subcritically unstable flows is the reduction in the critical shear rate from its value predicted by the linear theory (Γ_c), due the finite amplitude

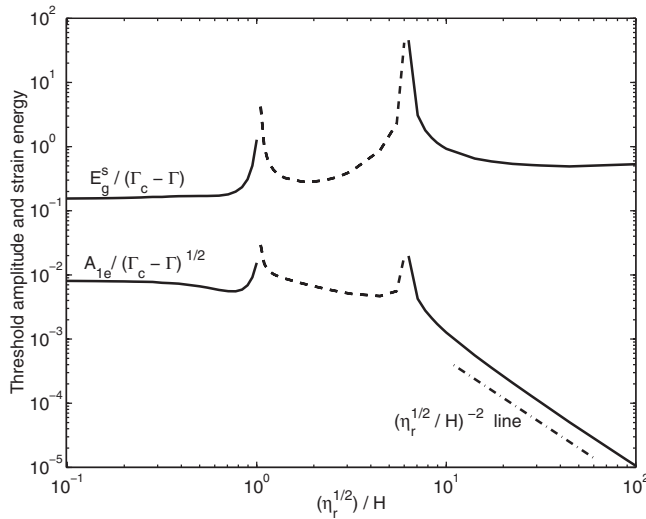


FIG. 9. Variation of the equilibrium amplitude $A_{1e}/\sqrt{\Gamma_c - \Gamma}$ and strain energy for the solid $E_g^s/(\Gamma_c - \Gamma)$ with $\sqrt{\eta_r}/H$ for $H=10$, $T=10$, and $De=0$. The threshold amplitude and energy are positive for the subcritical bifurcation and are negative for the supercritical bifurcation. For the later case, the quantities $A_{1e}/\sqrt{\Gamma - \Gamma_c}$ and $E_g^s/(\Gamma - \Gamma_c)$ and are plotted as broken lines.

nature of the disturbances. This reduction in Γ_c can be obtained from Eq. (51) by prescribing a particular level of disturbance amplitude. We take the normal displacement of the

fluid-solid interface as the representative quantity for the amplitude of the disturbance. The normal displacement of the interface, correct to $O(\epsilon)$, is given by

$$|u'_y|_{y=0} = A_{1e} |\bar{u}_y^{(1,1)}|_{y=0}. \quad (53)$$

Table II provides the percentage reduction in Γ from Γ_c for different levels of normal displacement of the interface. For $H=1$, $\eta_r=0$, and $T=0$, where the shortwave instability is critical, the reduction in critical shear rate is significant, as the finite amplitude nonlinear effects are strongly destabilizing. However, for the remaining set of parameters, where the critical mode is a finite wave-number mode, the finite amplitude disturbances do not result in a significant reduction in the critical shear rate required to destabilize the flow, when compared to the predictions of the linear stability theory. This result is consistent with the experimental observations [10], where the shear flow past a flexible surface was found to become unstable at a shear rate in the vicinity of the critical shear rate Γ_c predicted by the linear stability analysis.

The sign of $s_r^{(1)}$ varies with the parameters in an unpredictable manner. Hence, it is important to construct the regions indicating the sign of $s_r^{(1)}$. Figure 10(a) shows the different regions in the parametric space H versus $\sqrt{\eta_r}/H$ for $T=0$, clearly indicating the regions of subcritical instability ($s_r^{(1)} > 0$) as well as the regions of supercritical stability ($s_r^{(1)} < 0$). The values of Γ and α are kept at the critical point (α_c, Γ_c) corresponding to the values of the parameters at each point in this plot. The lower region of subcritical instability

TABLE II. Reduction in the critical velocity Γ required for instability when the flow is subcritical. Here Γ_c is the critical velocity obtained from the linear stability analysis and Γ is the critical velocity for the finite amplitude disturbance. Here, the normal displacement of the interface is taken as the representative of the perturbation amplitude. The Deborah number is kept zero.

	η_r	T	Interface displacement amplitude, $ u'_y _{y=0}$	% reduction in Γ $(\Gamma_c - \Gamma)/\Gamma_c \times 100$
$H=1$	0	0	0.001	0.8305
	0	0	0.010	83.049
	0	0	0.025	519.059
$H=10$	0	0	0.025	0.619
	0	0	0.050	2.476
	0	0	0.100	9.906
	0	10	0.025	0.547
	0	10	0.050	2.191
	0	10	0.100	8.766
	10	10	0.025	0.535
$H=100$	0	0	0.050	2.141
	0	0	0.100	8.562
	0	0	0.025	0.490
	0	0	0.050	1.959
	0	0	0.100	7.836
	100	100	0.025	0.521
	100	100	0.050	2.086
	100	100	0.100	8.344

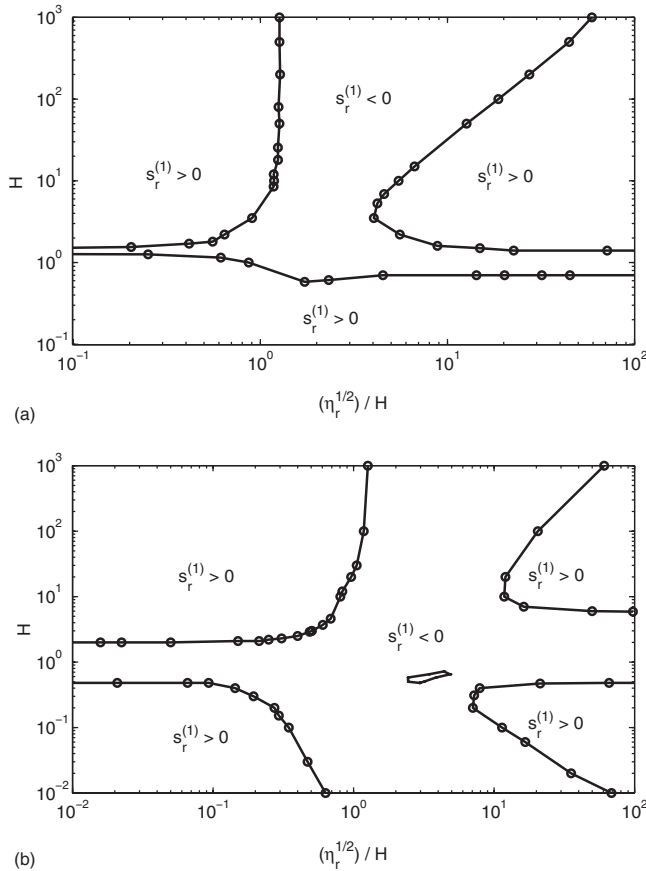


FIG. 10. The region marking the subcritical ($s_r^{(1)} > 0$) and supercritical ($s_r^{(1)} < 0$) bifurcation in the parametric space H versus $\sqrt{\eta_r}/H$. (a) $T=0$. (b) $T=100$. The Deborah number is kept zero.

is the region of upstream traveling shortwave modes, and in the remaining regions, the downstream traveling finite wave-number mode is the most critical. The crossover of the bifurcation from subcritical to supercritical upon increasing η_r is shown to occur at $\sqrt{\eta_r}/H \approx 1$. Figure 10(b) shows the similar plot for $T=100$. The stabilizing influence of the interfacial tension is evident, and the region of supercritical stability is wider than that for $T=0$.

V. CONCLUSIONS

The stability of the plane shear flow of a Newtonian fluid past an incompressible neo-Hookean solid in the limit of zero Reynolds number was studied using both the linear and weakly nonlinear stability analyses. While the linear stability analysis has been carried out before [1], an important new result of the present analysis is the effect of the relative viscosity of the elastic medium η_r on stability. For $\sqrt{\eta_r}/H < 1$, an increase in η_r results in an increase in Γ_c , reflecting the stabilizing influence of solid viscosity. In this regime, Γ_c scales as H^{-1} for $H \gg 1$. However, for $\sqrt{\eta_r}/H \approx 1$, the value of Γ_c attains a maximum, and any further increase in η_r results in a decrease in Γ_c in the regime $\sqrt{\eta_r}/H > 1$. The peak value of Γ_c scales as $H^{-1/2}$ for $H \gg 1$. This behavior for the neo-Hookean solid is significantly different from the analysis

of the linear viscoelastic solid [3], wherein the unstable mode ceases to exist for $\sqrt{\eta_r}/H > 1$ provided $\eta_r \geq 1$, as Γ_c diverges in the limit $\sqrt{\eta_r}/H \rightarrow 1$.

The weakly nonlinear analysis was carried out at the critical point to determine the nature of bifurcation. The first Landau constant $s^{(1)}$, whose real part provides the nonlinear correction to the linear growth rate, was calculated for a range of parameters. The sign of $s_r^{(1)}$ was found to be positive and large for the shortwave instability, indicating the bifurcation at the linear instability to be highly subcritical. The sign of $s_r^{(1)}$ for the finite wave-number instability mode was found to vary depending upon the parameters H , η_r , and T . This behavior is significantly different from that for the linearly elastic solid [21], for which the bifurcation always remained subcritical for a wide range of parameters, such as H and η_r . A plot in the parametric space H versus $\sqrt{\eta_r}/H$ was constructed to mark various regions of the subcritical instability and the supercritical stability for finite amplitude disturbances. The equilibrium amplitude and the threshold strain energy in the solid were also determined for finite amplitude disturbances in the vicinity of critical shear rate Γ_c . For the subcritically unstable flows, we also calculate the percent reduction in Γ from its value predicted by the linear stability theory Γ_c by prescribing the level of normal displacement at the interface. The reduction in the critical shear rate is about 83% for disturbances of amplitude 1% of the channel width R , for the shortwave instability. For the finite wave-number instability, the reduction in Γ is very small, up to about 1% for the perturbations with amplitude 2.5% of the channel width.

Thus, the present analysis highlights the important and counterintuitive destabilizing effect of solid viscosity on the stability, and shows that the flow past a neo-Hookean solid is more unstable than that past a linear elastic solid. There are, however, domains in parameter space where the bifurcation past a neo-Hookean solid is supercritical, in contrast to the subcritical nature of the bifurcation for the flow past a linear elastic solid. The results from this analysis provide a first step for designing systems to have a desired critical flow rate as well as a desired bifurcation in applications involving fluid flow past flexible solids in microfluidic applications.

APPENDIX: LAGRANGIAN DESCRIPTION

In this paper, we used the Eulerian (or spatial) description to formulate the dynamics of the viscoelastic solid, wherein the measurable quantities are defined at fixed points \mathbf{x} in space at a given time t . From the viewpoint of the particles, the spatial coordinates are the coordinates of the particles in the current deformed state. The dynamical variables are therefore expressed in terms of the deformed configuration. Alternately, the dynamical quantities can be expressed in terms of the material coordinates rather than the fixed spatial coordinates. Here, the reference position of the particles \mathbf{X} at an initial time $t=0$ is used to identify the particles at later time t . This reference configuration \mathbf{X} and time t form the independent variables in the Lagrangian (or referential) description. In this Appendix, we provide the set of governing equations for the neo-Hookean solid in Lagrangian frame-

work. The motion in the fluid is described in the Eulerian framework.

1. Problem formulation

Let $\mathbf{X}=(X_1, X_2, X_3)$ be the reference position, chosen as the initial unstressed state, of a particle X at time $t=0$. This particle X occupies the position $\mathbf{x}=(x_1, x_2, x_3)$ at a given time t . The subscripts (1, 2, 3) are used to indicate the position vector of the particle with respect to the fixed coordinate system (x, y, z) shown in Fig. 1. The motion of every particle in a continuum can be described generally by $\mathbf{x}=\mathbf{x}(\mathbf{X}, t)$. The displacement vector $\mathbf{u}=(u_1, u_2, u_3)$ of a particle from the reference position to the position at time t , is given by

$$\mathbf{u}(\mathbf{X}, t) = \mathbf{x}(\mathbf{X}, t) - \mathbf{X}. \quad (\text{A1})$$

An important kinematical quantity, the deformation gradient, is given by

$$\mathbf{F} = \frac{\partial \mathbf{x}}{\partial \mathbf{X}} = \mathbf{I} + \nabla_{\mathbf{X}} \mathbf{u}, \quad (\text{A2})$$

where the subscript \mathbf{X} indicates differentiation with respect to the reference configuration coordinates.

For the solid, the mass and the momentum conservation equations, written in the reference configuration, are

$$\text{Det } \mathbf{F} = 1, \quad (\text{A3})$$

$$\nabla_{\mathbf{X}} \cdot \boldsymbol{\sigma}^P = 0. \quad (\text{A4})$$

Above, Eq. (A3) is similar to the mass conservation equation in the Eulerian description [Eq. (6)], as $\mathbf{F} \cdot \mathbf{f} = \mathbf{I}$. Here, $\boldsymbol{\sigma}^P$ is the first Piola-Kirchhoff stress tensor. The constitutive equation for the neo-Hookean solid is

$$\boldsymbol{\sigma} = -p_g \mathbf{I} + 2\mathbf{e} + 2\eta_r \left(\frac{\partial \mathbf{e}}{\partial t} \right)_{\mathbf{X}=\text{fixed}}, \quad (\text{A5})$$

where $\boldsymbol{\sigma}$ is the Cauchy stress tensor. The strain tensor in Cauchy-Finger form is given by [13]

$$\mathbf{e} = \frac{1}{2}(\mathbf{F} \cdot \mathbf{F}^T - \mathbf{I}) \quad (\text{A6})$$

or

$$e_{ij} = \frac{1}{2} \left(\frac{\partial u_i}{\partial X_j} + \frac{\partial u_j}{\partial X_i} + \frac{\partial u_i}{\partial X_k} \frac{\partial u_j}{\partial X_k} \right). \quad (\text{A7})$$

The relationship between the first Piola-Kirchhoff stress tensor and the Cauchy stress tensor is given by

$$\boldsymbol{\sigma}^P = \mathbf{F}^{-1} \cdot \boldsymbol{\sigma}. \quad (\text{A8})$$

The particle velocity in material coordinates is simply the partial time derivative of the current position vector

$$\mathbf{v}^g = \left(\frac{\partial \mathbf{x}}{\partial t} \right)_{\mathbf{X}=\text{fixed}} = \frac{\partial \mathbf{u}}{\partial t}. \quad (\text{A9})$$

The steady shear flow with strain rate Γ past a neo-Hookean solid induces deformation of the elastic continuum

from its initial configuration $\mathbf{X}=(X_1, X_2, X_3)$ to $\bar{\mathbf{x}}=(\bar{x}_1, \bar{x}_2, \bar{x}_3)$ given by

$$\bar{\mathbf{x}} = [\Gamma(X_2 + H) + X_1, X_2, X_3], \quad (\text{A10})$$

$$\bar{\mathbf{u}} = [\Gamma(X_2 + H), 0, 0] \quad \text{and} \quad \bar{\mathbf{v}}^g = (0, 0, 0). \quad (\text{A11})$$

The base-state stresses in the solid medium are

$$\bar{\sigma}_{11} = -\bar{p}_g + \Gamma^2, \quad \bar{\sigma}_{12} = \Gamma, \quad \bar{\sigma}_{22} = -\bar{p}_g. \quad (\text{A12})$$

2. Stability analysis

The formulation of the stability problem with perturbation deformations superimposed on a base-state deformation is briefly discussed next. Let B_0 denote the initial unstressed elastic body with the position vector of a representative particle given by \mathbf{X} . By shearing the fluid resting above the solid, a static deformation is imposed upon B_0 resulting in a finitely stressed equilibrium (base) configuration denoted by B_e . In this state, the position vector of a particle which was initially at \mathbf{X} is denoted by $\bar{\mathbf{x}}(\mathbf{X})$. The particle displacement from state B_0 to B_e is given by $\bar{\mathbf{u}}(\mathbf{X}) = \bar{\mathbf{x}}(\mathbf{X}) - \mathbf{X}$ and the deformation gradient is $\bar{\mathbf{F}} = (\partial \bar{\mathbf{x}} / \partial \mathbf{X})$. Now, a time-dependent perturbation wave is superimposed on B_e and the resulting configuration, referred to as the current configuration, is denoted by B_t . The position vector of a representative particle in configuration B_t is denoted by $\mathbf{x}(\mathbf{X}, t) = (x_1, x_2, x_3)$. We may express $\mathbf{x}(\mathbf{X}, t) = \bar{\mathbf{x}}(\mathbf{X}) + \mathbf{u}'(\bar{\mathbf{x}}, t)$, where $\mathbf{u}'(\bar{\mathbf{x}}, t) = (u'_1, u'_2, u'_3)$ is the perturbation particle displacement associated with the deformation $B_e \rightarrow B_t$. The deformation gradient arising from this deformation is $\mathbf{F}' = (\partial \mathbf{x} / \partial \bar{\mathbf{x}}) = (\mathbf{I} + \partial \mathbf{u}' / \partial \bar{\mathbf{x}})$. The overall deformation gradient generated by the deformation $B_0 \rightarrow B_t$ is

$$\mathbf{F} = \frac{\partial \mathbf{x}}{\partial \mathbf{X}} = \frac{\partial \mathbf{x}}{\partial \bar{\mathbf{x}}} \cdot \frac{\partial \bar{\mathbf{x}}}{\partial \mathbf{X}} = \mathbf{F}' \cdot \bar{\mathbf{F}} = \left(\mathbf{I} + \frac{\partial \mathbf{u}'}{\partial \bar{\mathbf{x}}} \right) \cdot \left(\mathbf{I} + \frac{\partial \bar{\mathbf{u}}}{\partial \mathbf{X}} \right). \quad (\text{A13})$$

The incompressibility constraint is $\text{Det } \mathbf{F} = 1$. The equation of motion takes the form

$$\nabla_{\bar{\mathbf{x}}} \cdot \boldsymbol{\sigma}^P = 0. \quad (\text{A14})$$

The first Piola-Kirchhoff stress tensor is given by

$$\boldsymbol{\sigma}^P = \mathbf{F}'^{-1} \cdot \boldsymbol{\sigma}, \quad (\text{A15})$$

$$\boldsymbol{\sigma} = -p_g \mathbf{I} + (\mathbf{F} \cdot \mathbf{F}^T - \mathbf{I}) + \eta_r \partial_t (\mathbf{F} \cdot \mathbf{F}^T - \mathbf{I}). \quad (\text{A16})$$

Here, the Deborah number for solid is taken zero for simplicity.

In weakly nonlinear theory, we seek the solution in the form of harmonics of the fundamental wave, each one expanded in amplitude series. Using the definition $E(\bar{x}_1, t) = \exp[i(\alpha \bar{x}_1 + \omega t)]$ for convenience, a general quantity ϕ , pertaining to the elastic solid, is expanded as follows:

$$\phi(\mathbf{X}, t) = \bar{\phi}(\mathbf{X}) + \phi'(\bar{\mathbf{x}}, t), \quad (\text{A17})$$

TABLE III. Comparison of the results from the Eulerian and the Lagrangian descriptions: The Landau constant $s^{(1)}$ for different values of H keeping $\eta_r=0$ and $T=0$.

H	α_c	Γ_c	Eulerian framework		Lagrangian framework	
			Real[$s^{(1)}$]	Imag[$s^{(1)}$]	Real[$s^{(1)}$]	Imag[$s^{(1)}$]
0.10	100.0	2.93114248	253529.143	56714.095	253556.630	56613.743
0.50	29.20	2.93114246	21546.593	4599.1451	21546.497	4599.1673
1.00	17.64	2.93114246	7837.8850	1598.3704	7837.8801	1598.2711
1.20	17.34	2.93114246	7572.5541	1540.9946	7572.5998	1541.1194
1.27	0.620	2.91813557	-18.5149687	-43.2588194	-18.5149725	-43.2588039
1.50	0.630	2.27140715	-2.0288370	-29.2209990	-2.0288389	-29.2210017
2.00	0.614	1.54046549	11.7108298	-15.2426429	11.7108249	-15.2426526
5.00	0.355	0.57410443	39.7070800	-3.2991380	39.7070791	-3.2991424
10.00	0.178	0.29680357	92.1882493	-22.1699354	92.1882171	-22.1699473
50.00	0.0331	0.06268374	362.255355	-293.713077	362.255268	-293.713036
100.0	0.0163	0.03162049	674.548152	-612.078718	674.548055	-612.078210
1000	0.0016	0.00318887	6300.04658	-6379.19398	6300.04654	-6379.1943

$$\phi'(\bar{\mathbf{x}}, t) = \sum_{k=0}^{\infty} \sum_{n=k, n \neq 0}^{\infty} [A_1(\tau)]^n [E^k \tilde{\phi}^{(k,n)}(\bar{\mathbf{x}}_2) + E^{-k} \tilde{\phi}^{(k,n)\dagger}(\bar{\mathbf{x}}_2)], \quad (\text{A18})$$

where the superscript \dagger denotes the complex conjugate, and $\phi = [\mathbf{u}, p_g]$.

Apart from the no-slip condition at the bottom plate, $u'_1(-H) = u'_2(-H) = 0$, we need boundary conditions at the fluid-solid interface. Denoting F and G as the fluid and the solid quantities, respectively, the interface condition can be symbolically written as

$$F(x, y, t)|_{x+\xi, \eta} = G(\bar{x}_1, \bar{x}_2, t)|_{\bar{x}_1+\xi, \eta}, \quad (\text{A19})$$

where ξ and η are the horizontal and the vertical displacement of the material coordinates of a particle at the interface (see Fig. 2); that is, $\xi = u'_1|_{\bar{x}_2=0}$ and $\eta = u'_2|_{\bar{x}_2=0}$. As the Eulerian description is used for the fluid flow, the left side of Eq. (A19) is expressed by a Taylor series expansion about the flat interface, as explained in Sec. III. For the gel side, material coordinates are used such that any quantity is expressed in terms of coordinates of the particles in base configuration B_e . Therefore, the right side of the above equation is simply given by

$$G(\bar{x}_1, \bar{x}_2, t)|_{\bar{x}_1+\xi, \eta} = G(\bar{x}_1 = x, \bar{x}_2 = 0, t). \quad (\text{A20})$$

The Taylor series expansion is not needed to evaluate any gel quantity on the perturbed interface in the material description.

Finally, we provide the equations for the linear stability problem as follows:

$$i\alpha \tilde{u}_1^{(1,1)} + d_{\bar{x}_2} \tilde{u}_2^{(1,1)} = 0,$$

$$-i\alpha \tilde{p}_g^{(1,1)} + (1 + s^{(0)} \eta_r)(d_{\bar{x}_2}^2 \tilde{u}_1^{(1,1)} - \alpha^2 \tilde{u}_1^{(1,1)} - \alpha^2 \Gamma^2 \tilde{u}_1^{(1,1)}) + 2i\alpha \Gamma d_{\bar{x}_2} \tilde{u}_1^{(1,1)} = 0,$$

$$-d_{\bar{x}_2} \tilde{p}_g^{(1,1)} + (1 + s^{(0)} \eta_r)(d_{\bar{x}_2}^2 \tilde{u}_2^{(1,1)} - \alpha^2 \tilde{u}_2^{(1,1)} - \alpha^2 \Gamma^2 \tilde{u}_2^{(1,1)}) + 2i\alpha \Gamma d_{\bar{x}_2} \tilde{u}_2^{(1,1)} = 0.$$

The above equations are supplemented with the boundary conditions $\tilde{u}_1^{(1,1)}(-H) = \tilde{u}_2^{(1,1)}(-H) = 0$, and the following interface conditions to be applied at $\bar{x}_2 = y = 0$:

$$\tilde{v}_y^{(1,1)} = s^{(0)} \tilde{u}_2^{(1,1)},$$

$$\tilde{v}_x^{(1,1)} + \Gamma \tilde{u}_2^{(1,1)} = s^{(0)} \tilde{u}_1^{(1,1)},$$

$$d_y \tilde{v}_x^{(1,1)} + i\alpha \tilde{v}_y^{(1,1)} = (1 + s^{(0)} \eta_r)(d_{\bar{x}_2} \tilde{u}_1^{(1,1)} + i\alpha \tilde{u}_2^{(1,1)} + i\alpha \Gamma^2 \tilde{u}_2^{(1,1)}) - i\alpha \Gamma^2 \tilde{u}_2^{(1,1)},$$

$$-\tilde{p}_f^{(1,1)} + 2d_y \tilde{v}_y^{(1,1)} = -\tilde{p}_g^{(1,1)} + 2(1 + s^{(0)} \eta_r)(d_{\bar{x}_2} \tilde{u}_2^{(1,1)} + i\alpha \Gamma \tilde{u}_2^{(1,1)}) + T\alpha^2 \tilde{u}_2^{(1,1)}.$$

The sequential solution of the problems at various orders leads to the first Landau constant $s^{(1)}$. While the expressions for the various quantities such as the solid velocity and the implementation of the interface conditions are grossly different from the corresponding expressions in the Eulerian description, the results using the Lagrangian description are identical with those obtained using the Eulerian description for the solid dynamics. The agreement between the results from both the descriptions is shown in Table III.

- [1] V. Gkanis and S. Kumar, *Phys. Fluids* **15**, 2864 (2003).
- [2] P. Krindel and A. Silberberg, *J. Colloid Interface Sci.* **71**, 39 (1979).
- [3] V. Kumaran, G. H. Fredrickson, and P. Pincus, *J. Phys. II* **4**, 893 (1994).
- [4] V. Kumaran, *J. Fluid Mech.* **294**, 259 (1995).
- [5] V. Kumaran, *J. Fluid Mech.* **320**, 1 (1996).
- [6] L. Srivatsan and V. Kumaran, *J. Phys. II* **7**, 947 (1997).
- [7] V. Kumaran, *J. Fluid Mech.* **357**, 123 (1998).
- [8] V. Kumaran, *J. Fluid Mech.* **362**, 1 (1998).
- [9] V. Kumaran and R. Muralikrishnan, *Phys. Rev. Lett.* **84**, 3310 (2000).
- [10] R. Muralikrishnan and V. Kumaran, *Phys. Fluids* **14**, 775 (2002).
- [11] M. D. Eggert and S. Kumar, *J. Colloid Interface Sci.* **278**, 234 (2004).
- [12] L. E. Malvern, *Introduction to the Mechanics of a Continuous Medium* (Prentice-Hall, Englewood Cliffs, NJ, 1969).
- [13] C. W. Macosko, *Rheology: Principles, Measurements, and Applications* (VCH, New York, 1994).
- [14] Y. Renardy, *J. Non-Newtonian Fluid Mech.* **28**, 99 (1988).
- [15] V. Gkanis and S. Kumar, *J. Fluid Mech.* **524**, 357 (2005).
- [16] V. Gkanis and S. Kumar, *Phys. Fluids* **18**, 044103 (2006).
- [17] S. A. Roberts and S. Kumar, *J. Non-Newtonian Fluid Mech.* **139**, 93 (2006).
- [18] J. Adepun and V. Shankar, *J. Non-Newtonian Fluid Mech.* **141**, 43 (2007).
- [19] J. T. Stuart, *J. Fluid Mech.* **9**, 353 (1960).
- [20] J. Watson, *J. Fluid Mech.* **9**, 371 (1960).
- [21] V. Shankar and V. Kumaran, *J. Fluid Mech.* **434**, 337 (2001).
- [22] N. Phan-Thien, *J. Non-Newtonian Fluid Mech.* **95**, 343 (2000).
- [23] R. M. Thaokar and V. Kumaran, *J. Fluid Mech.* **472**, 29 (2002).